NEW MORPHOMETRIC MEASUREMENTS OF PEAK-RING BASINS ON MERCURY AND THE MOON: RESULTS FROM THE MERCURY LASER ALTIMETER AND LUNAR ORBITER LASER ALTIMETER. David M.H. Baker[1], James W. Head[1], Louise M. Prockter[2], Caleb I. Fassett[3], Gregory A. Neumann[4], David E. Smith[4,5], Sean C. Solomon[6], Maria T. Zuber[4,5], Jürgen Oberst[7], Frank Preusker[7], and Klaus Gwinner[7]; [1]Dept. Geological Sci., Brown Univ., Box 1846, Providence, RI 02912, Email: David_Baker@brown.edu, [2]Johns Hopkins University Applied Physics Laboratory, Laurel, MD 20723, [3]Dept. of Astronomy, Mount Holyoke College, South Hadley, MA 01075, [4]Solar System Exploration Division, NASA Goddard Space Flight Center, Greenbelt, MD 20771, [5]Department of Earth, Atmospheric and Planetary Sciences, MIT, Cambridge, MA 02139, [6]Department of Terrestrial Magnetism, Carnegie Institution of Washington, Washington, DC 20015, [7]German Aerospace Center (DLR), Rutherfordstr. 2, Institute of Planetary Research, D-12489 Berlin, Germany.

Introduction: Peak-ring basins (large impact craters exhibiting a single interior ring) are important to understanding the processes controlling the morphological transition from craters to large basins on planetary bodies. New image and topography data from the MErcury Surface, Space ENvironment, GEochemistry, and Ranging (MESSENGER) and Lunar Reconnaissance Orbiter (LRO) spacecraft have helped to update the catalogs of peak-ring basins on Mercury and the Moon [1,2] and are enabling improved calculations of the morphometric properties of these basins. We use current orbital altimeter measurements from the Mercury Laser Altimeter (MLA) [3] and the Lunar Orbiter Laser Altimeter (LOLA) [4], as well as stereo-derived topography [5], to calculate the floor depths and peak-ring heights of peak-ring basins on Mercury and the Moon. We present trends in these parameters as functions of rim-crest diameter, which are likely to be related to processes controlling the onset of peak rings in these basins.

Methods: All morphometric calculations use the freshest basins in current catalogs [1,2]. The lack of coverage of stereo-derived topography and MLA tracks in the southern hemisphere due to MESSENGER's highly elliptical orbit restricted analysis of basins on Mercury to the northern hemisphere. Two methods were employed. The first (Fig. 1a) was a semi-automated technique using gridded Digital Elevation Models (DEMs) from LOLA at ~236 m/pixel (Moon) [4] and DEMs at 1 km/pixel derived from stereo-photogrammetry of MESSENGER flyby images [5] (Mercury). Topographic data were extracted from the DEMs along radial transects extending outward from the center of the basin to 3.5 basin radii and separated by 1° azimuthal intervals. Maximum elevation values were then extracted within pre-defined buffer zones for the rim crest, base of the rim wall, peak ring, and basin center. From these values, we calculated a number of morphometric parameters for an individual profile, including basin depth, height of the peak ring, and wall height and slope. A single value for a parameter, such as basin depth (Fig. 2a), was determined by calculating the median and interquartile range (i.e. the central 50% of the population) of the set of all profile measurements. This technique also excluded those regions affected by superposed craters or proximal erosion ("EZ" in Fig. 1a).

The second method (Fig. 1b) used individual shot data from MLA [3]. We used this technique for basins on Mercury because of the large spacing between altimeter tracks over most of the basins, which precluded use of gridded DEMs. Two or more tracks traversing the basin, with at least one traversing the center of the basin, were required for measurement. All returned shots were first filtered on the basis of MLA receiver-channel noise thresholds [6]. From a Mercury Dual Imaging System (MDIS) global monochrome mosaic, we then digitized the outlines of the rim crest, base of the rim wall, crest of the peak ring, and inner boundary between the peak ring and the basin floor (i.e., the "center polygon"). All MLA shot points within 1 km of the outlines were then extracted for use in calculating median and interquartile range values for the elevations of the rim crest, base of the rim wall, and peak ring. We calculated the elevation of the center of the basin as the median and interquartile range of MLA shot data falling completely within the center polygon. This technique is limited by the density and locations of MLA tracks over each basin and the accuracy of identifying basin features from monochrome images. All of the data in the analysis are referenced to spheres of radius 1737.5 km for the Moon and 2440 km for Mercury.

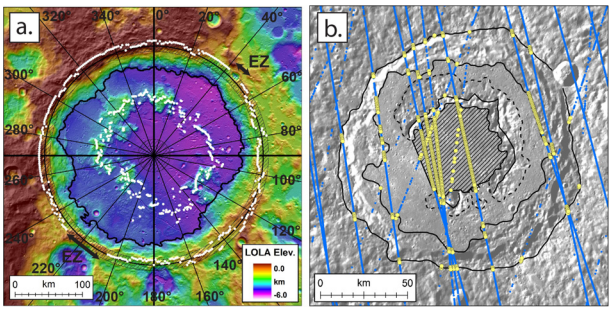

Fig. 1. Methods of morphometric measurements. (a) Extraction of maximum elevation points (white points) from DEMs along radial profiles [LOLA topography of Schrödinger basin on the Moon (326 km diameter, 74.90°S, 133.09°E)]. (b) Extraction of all elevation points (yellow points) from individual altimeter shots (blue points) that fall within a 1 km distance of digitized outlines of basin features (solid black lines) [MDIS mosaic of Ahmad Baba on Mercury (124 km diameter, 58.26°N, 231.48°E)]. North is toward the top in each image.

Results: Eight peak-ring basins on the Moon and eleven on Mercury were analyzed. We observe general agreement between calculations from MLA and stereo-derived DEMs for the same basins on Mercury [Figs. 2,3], supporting use of both techniques in our analysis. Among multiple morphometric parameters calculated, we focus our attention on the trends in depth and height of the peak ring as a function of diameter.

(1) Depth (d) versus diameter (D_r): Williams and Zuber (1998) [8] derived a power-law relation between depth (d) and diameter (D_r) for peak-ring and multi-ring basins on the Moon that was shallower than the trend for complex craters [9,10], indicating a transition to relatively smaller d/D_r ratios from complex craters to basins. Our d versus D_r data for the Moon (Fig. 2a) support the conclusion that peak-ring basins have smaller d/D_r ratios. However, our data for both Mercury and the Moon indicate steeper power law trends for peak-ring basins than inferred previously [$d = (0.039\pm0.040)(D_r)^{0.83\pm0.19}$, R^2=0.88 (Mercury) and $d = (0.35\pm1.0)(D_r)^{0.44\pm0.48}$, R^2=0.37 (Moon)]. These trends suggest that there is a decrease of ~40%

in crater depth in the transition between complex craters and peak-ring basins. Possible reasons for this decrease include an increase in floor uplift associated with peak ring formation, reduced cratering efficiency [11], increased retention of impact melt [12], viscous relaxation [13], or a combination of these process. The relative importance of each of these processes is still being considered, although the step-wise decrease in depth between complex craters and peak-ring basins suggest that it is most likely related to the cratering process, such as formation of peak rings.

We also observe a general decrease in the depth/diameter ratio for peak-ring basins on Mercury and the Moon (Fig. 2b). Again, this decrease may result from a number of factors, including decrease in cratering efficiency, increase in impact melt retention, or viscous relaxation. Basins on Mercury also have slightly smaller d/Dr ratios for a given diameter than does the Moon, which may be a function of global differences in thermal evolution, surface gravitational acceleration, or target properties.

(2) Peak-ring height (h_{pr}) versus diameter (D_r): There is a general increase in the height of the peak ring (h_{pr}) as a function of rim-crest diameter (D_r) on the Moon and Mercury (Fig. 3a), which appears similar to the trends of central peak heights in complex craters [9,14]. The great scatter in the data, especially for Mercury, is due to the highly irregular nature of peak-ring topography and also biases introduced by the current sparseness of MLA tracks. Despite the scatter, we find that h_{pr} values on Mercury are generally larger than on the Moon. This is also shown in a plot of h_{pr}/d ratios (Fig. 3b), which increase from 0.1 to 0.7 over the range of peak-ring basin diameters. The larger h_{pr} values on Mercury are likely to be the result of the combined effects of higher mean impactor velocities at Mercury (~40 km/s versus ~20 km/s) [15] and Mercury's higher gravitational acceleration (~3.7 m/s^2 versus ~1.6 m/s^2), which may act to enhance collapse of the transient cavity.

Summary: We used two new techniques for calculating the morphometric properties of peak-ring basins on Mercury and the Moon from recent data acquired by the Mercury Laser Altimeter and Lunar Orbiter Laser Altimeter. We derived new trends in basin depths and heights of peak rings as functions of increasing rim-crest diameter, although many more parameters, including wall height and slope, rim-flank height, and floor height and radii have been calculated. Future extension of these measurements to other transitional basins, such as protobasins, will help to elucidate these trends and our understanding of the processes controlling the transitions with increasing diameter from complex craters to peak-ring basins and to multi-ring basins.

References: [1] Baker, D.M.H. et al. (2011a) *Icarus*, 214, 377-393. [2] Baker, D.M.H. et al. (2011b) *Planet. Space Sci.*, 59, 1932-1948. [3] Zuber, M.T. et al. (2008) *Science*, 321, 77-79. [4] Smith, D.E. et al. (2010) *Geophys. Res. Lett.*, 37, L18204. [5] Preusker, F. et al. (2011) *Planet. Space Sci.*, 59, 1910-1917. [6] Cavanaugh, J.F. et al. (2007) *Space Sci. Rev.*, 131, 451-479. [8] Williams, K.K. and M.T. Zuber (1998) *Icarus*, 131, 107-122. [9] Pike. R.J. (1977) in *Impact and Explosion Cratering*, Roddy, D.J. et al. (eds.), Pergamon Press, New York., pp. 489–509. [10] Pike, R.J. (1988) in *Mercury*, Vilas, F. et al. (eds.), Univ. Arizona Press, pp. 165-273. [11] Melosh, H.J. (1989) *Impact Cratering: A Geological Process*, Oxford Univ. Press, London. [12] Cintala, M.J. and R.A.F. Grieve (1998) *Meteorit. Planet. Sci.*, 33, 889-912. [13] Mohit, P.S. et al. (2009) *Earth Planet. Sci. Lett.*, 285, 355-363. [14] Hale, W.S. and R.A.F. Grieve (1982) *J. Geophys. Res.*, 87, A65-A76. [15] Le Feuvre, M. and M.A. Wieczorek (2008) *Icarus*, 197, 291-306.

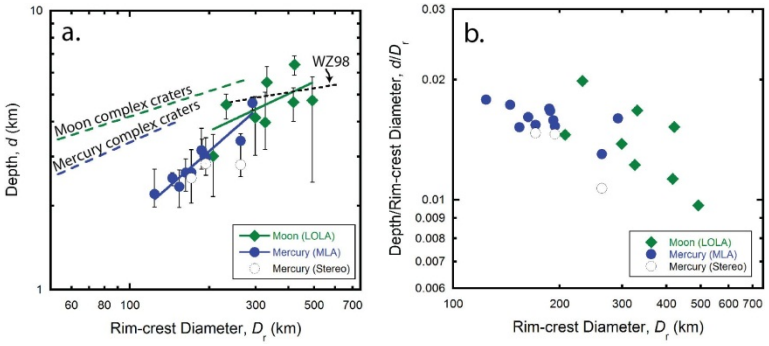

Fig. 2. Log-log plots of depth (a) and the ratio of depth to rim-crest diameter (b) vs. rim-crest diameter for peak-ring basins on Mercury (measurements from MLA, blue circles, and stereo topography, open circles) and the Moon (green diamonds). All points are median values and error bars show interquartile ranges (i.e., the central 50% of the populations). Solid lines are power-law fits to the data, given in the text. Trends for basin measurements [8] (WZ98) and complex craters on Mercury [10] and the Moon [9] are shown as dashed lines in (a).

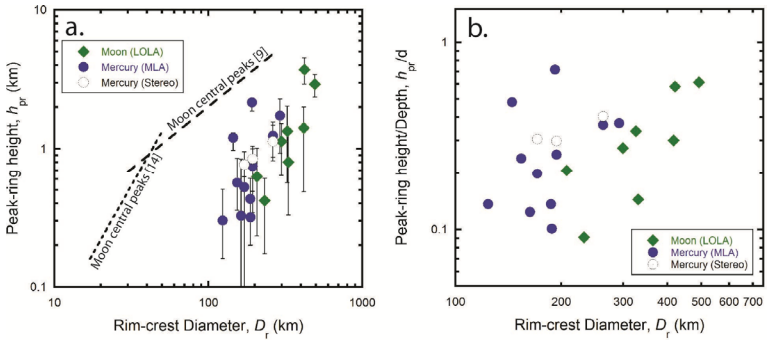

Fig. 3. Log-log plots of peak-ring height (a) and the ratio of peak-ring height to rim-crest diameter (b) vs. rim-crest diameter for peak-ring basins on Mercury (measurements from MLA, blue circles, and stereo topography, open circles) and the Moon (green diamonds). All points are median values and error bars show interquartile ranges. Trends for the heights of central peaks in complex craters on the Moon [9,14] are shown as dashed lines in (a); such trends have not been determined for Mercury [10].